Natriuretic peptides protect against apoptosis and increase cGMP around cardiomyocyte mitochondria

Gaia Calamera[1], Bernadin Ndongson-Dongmo[1], Dulasi Arunthavarajah[1], Mette Ovesen[1], Choel Kim[2, 3], Finn Olav Levy[1†], Kjetil Wessel Andressen[1*] and Lise Román Moltzau[1*].

[1]Department of Pharmacology, Institute of Clinical Medicine, University of Oslo and Oslo University Hospital, P.O. Box 1057 Blindern, 0316 Oslo, Norway

[2]Department of Pharmacology and Chemical Biology, Baylor College of Medicine, Houston, TX, USA

[3]Verna and Marrs McLean Department of Biochemistry and Molecular Biology, Baylor College of Medicine, Houston, TX, USA

*shared senior author

[†] Corresponding Author: Finn Olav Levy, Department of Pharmacology, Faculty of Medicine, University of Oslo, Sognsvannsveien 20, P.O.Box 1057 Blindern, N-0316 Oslo, Norway. Tel: +47 22840237. Fax: +47 22840202. E-mail: f.o.levy@medisin.uio.no

Abstract

Natriuretic peptides (NPs) increase cGMP, show beneficial cardiovascular effects and has been shown to regulate energy metabolism in other tissues. However, little is known about their direct effect on cardiac mitochondria and cardiomyocyte apoptosis. Here, we examined whether NPs increase cGMP around mitochondria and alter apoptosis in cardiomyocytes. Stimulating with ANP or CNP reduced apoptosis, together with reduced caspase 9 activation and cytochrome c release, suggesting that NPs decrease apoptosis through the intrinsic pathway that involves mitochondria. We engineered a novel FRET-based biosensor with high selectivity towards cGMP and targeted this to the outer mitochondrial membrane (OMM) and found that ANP and CNP increase cGMP at the OMM. Moreover, ANP and CNP increased phosphorylation of the pro-apoptotic protein Drp1 and CNP prevented fragmentation of mitochondria. We suggest that cGMP increase in the OMM microdomain inhibits the pro-apoptotic protein Drp1, leading to reduced mitochondrial fragmentation that inhibits apoptosis.

Introduction

Heart failure is associated with an imbalance in cell energy, changes in the energy source and oxidative stress[1-3]. In addition to providing ATP for the contraction mechanism in cardiomyocytes, mitochondria are also important in regulation of cellular metabolism, cell differentiation, motility, intracellular Ca^{2+} signaling and apoptosis[4,5]. The signaling molecule cGMP has been shown to induce mitochondrial potassium channel opening, mediating a beneficial effect in ischemia-reperfusion injury[6-10]. Natriuretic peptides (NP) increase cGMP by activation of the particulate guanylyl cyclase (pGCs). Atrial (ANP) and brain NP (BNP) both activate the NP receptor GC-A while C-type NP (CNP) activates GC-B. NPs can mediate several beneficial effects in the cardiovascular system such as diuresis, natriuresis, vasodilation and antihypertrophic effects[11]. Consequently, recent attention has been given to drugs that increase NP levels as potential treatment of heart failure. Sacubitril-valsartan, a neprilysin (NEP) inhibitor in combination with an AT_1 angiotensin II receptor antagonist, was shown to be superior to the angiotensin converting enzyme inhibitor enalapril in the treatment of heart failure with reduced ejection fraction (HFrEF)[12]. The role of NPs in heart disease still needs to be better understood to further improve treatments. Natriuretic peptides have been shown to regulate cell metabolism and be beneficial against metabolic disease[13], but little is known about direct effects of NPs on mitochondrial function in the heart.

Hence, our aim was to investigate whether NPs can modulate mitochondrial function in the heart and whether NPs specifically increase cGMP in nanodomains surrounding the mitochondria. In the present study, we show that both CNP and ANP protect from apoptosis, confirmed by reduced Poly (ADP-ribose) polymerase (PARP) cleavage, and we show reduced cytochrome c release from mitochondria and reduced caspase 9 activation, suggesting that the apoptosis involves the mitochondrial pathway. We also show that NPs can increase phosphorylation of Drp1 and CNP can prevent mitochondrial fragmentation, which can mediate an anti-apoptotic effect. Finally, we developed a novel FRET-based biosensor selective for cGMP and confined this to the outer mitochondrial membrane (OMM) that allowed us to detect local cGMP increases from both ANP and CNP in real time in intact cells.

Materials and Methods

Materials. Human C-Type natriuretic peptide (CNP) and rat atrial natriuretic peptide (ANP) were from GenScript Corp. (Piscataway, NJ, USA). Mitotracker Deep Red, Mitotracker Green, Dulbecco's modified Eagle's medium (DMEM) with GlutaMAX, sodium pyruvate and MEM NEAA were from ThermoFisher Scientific. All other chemicals and media were from Sigma-Aldrich (Sigma-Aldrich, St.Louis, MO), unless otherwise specified.

Animals. This investigation was approved by the Norwegian Food Safety Authority (application number 8683 and 23286) and conforms to the research animal Directive 2010/63/EU, the Guide for the Care and Use of Laboratory Animals (NIH publication No. 85-23, revised 2011, US), in accordance with the ARRIVE guidelines[14]. Animals were anaesthetized in 4-5 % isoflurane and anesthesia was confirmed by abolished pain reflexes. Animals were euthanized by cervical dislocation and the chest was then opened to extract the heart.

Isolation of cardiomyocytes. Primary culture of cardiac ventricular myocytes from male Wistar rats were prepared as previously described[15].

LDH measurements. Cell death was measured by the LDH-Glo™ Cytotoxicity Assay (Promega, Mannheim, Germany). Cardiomyocytes cultured for 20 h were stimulated with CNP (1 μM), ANP (1 μM) or vehicle (H_2O) at time 0. Medium was sampled at the indicated time (0, 3, 6, 12 and 24 h) and added to LDH storage buffer (200 mM Tris-HCl pH 7.4, 10% glycerol, 1% BSA). Measurements were performed according to manufacturer's instructions.

ATP assay. Cardiomyocyte viability was measured as changes in cellular ATP levels using the CellTiter-Glo® 2.0 Cell Viability Assay (Promega). Cardiomyocytes cultured for 20 h were stimulated with CNP (1 μM), ANP (1 μM) or vehicle (H_2O). After 3 and 24 h from stimulation, cardiomyocytes were washed with 50 mM Tris-HCl pH 7.4, 150 mM NaCl, 2 mM EDTA and lysed using Solobuffer cell lysis kit (Fabgennix, Frisco, TX 75033, US). Measurements of ATP in the samples were performed according to manufacturer's instructions. Change in cellular ATP content after each stimulation time was calculated as (ATP in treated cells)/(ATP in vehicle-treated).

TUNEL assay. After 20 h from plating, adult cardiomyocytes were stimulated with either CNP (1 μM), ANP (1 μM) or vehicle (H_2O) for 3 h. To detect apoptotic cells, the ApopTag Plus Fluorescein In Situ Apoptosis Detection Kit (Merck, Darmstadt, Germany) was used according to the manufacturer's protocol. DAPI (5μg/ml) was added for nuclear staining. Cells were

visualized under an Olympus BX53 (Olympus, Japan), using an air objective (10x, 0.30NA, Olympus), and images taken with a XC50 color camera and cellSens Entry Software (Olympus, Japan). Images were acquired and analysed by a blinded operator.

Immunoblot analysis. Cardiomyocytes cultured for 20 h were stimulated with CNP (1 μM), ANP (1 μM) or vehicle (H_2O). After 3 h stimulation, protein was extracted on ice using lysis buffer (Tris 50 mM, EDTA 1 mM, EGTA 1 mM, NaF 50 mM, DTT 1 mM, $Na_4P_2O_7$ 10 mM, Na_3VO_4 1 mM, Triton X- 100 0.01%, SDS 0.05% and deoxycholat 0.5 %) supplemented with protease inhibitor cocktail and PMSF (1 mM). Samples were solubilized in loading buffer (62.5 mM Tris-HCl, glycerol 10%, bromophenol blue 1% wt/vol, SDS 2%, mercaptoethanol 2.5%) and denatured for 5 min at 95°C. Protein samples were separated by SDS-PAGE using 6%, 7.5% or 15% polyacrylamide gels and then transferred to a PVDF membrane. Membranes were blocked with 3% non-fat dry milk in Tris-buffered saline containing Tween-20 (0.1%) for 2 h and then incubated with the indicated primary antibodies overnight at 4°C, followed by incubation with appropriate secondary antibodies for 1 h at room temperature. Drp1 expression was quantified using a nitrocellulose membrane previously probed with pDrp1 S637. The membrane was stripped for 10 min in stripping solution (Glycine 0.15% w/v, SDS 0.1% w/v, Tween-20 1%, pH 2.2), then washed with phosphate-buffered saline and Tris-buffered saline containing Tween-20 (0.1%). The membrane was then blocked and incubated with Drp1 primary antibody followed by appropriate secondary antibody as described above. Blots were developed by enhanced chemiluminescence reaction using an Epi Chemi II Darkroom with Labworks Software (UVP Laboratory Products, Cambridge, UK). Protein expression or protein phosphorylation was quantified as measured intensity of area under the curve in ImageJ software. The intensity of each band was normalized to the intensity of the corresponding loading control (vinculin) except for cleaved PARP that was normalised to total PARP (cleaved+uncleaved). Antibodies: Vinculin (1:5000), PARP (1:1000), Cleaved PARP (1:800), Caspase 9 (1:1000), Phospho Drp1 S637 (1:100), Drp1 (1:1000), all from Cell Signaling.

Cytoplasmic cytochrome c release. Adult cardiomyocytes were cultured for 20 h and then treated with CNP (1 μM), ANP (1 μM) or vehicle (H_2O) for 3 h, washed twice with 50 mM Tris-HCl pH 7.4, 150 mM NaCl, 2 mM EDTA, incubated on ice with "cytoplasmic extraction buffer" from Subcellular Protein Fractionation Kit (Thermo Scientific, Waltham, USA) for 15 min, cells were then scraped and samples collected and centrifuged at 4 °C for 5 min at 500 x g. The supernatant (cytoplasmic fraction) was further centrifuged at 13000 x g for 10 min to separate the mitochondria (and other organelles). The supernatant was then collected and

126 cytochrome c measured using cytochrome c ELISA Kit (MyoBiosource, San Diego, USA)
127 following the manufacturer's instructions.

128 **Construction of FRET-based biosensors for cGMP.** The sequences encoding cGi-500V and
129 ScGI sensors were synthesized by GenScript and inserted into the vector pcDNA3.1(-). cGi-
130 500V sequence was from *Bos Taurus* PKG I (Gln^{79}-Tyr^{345}) flanked by CFP and Venus. The
131 ScGI sequence differs only by the mutation Cys158Arg. The OMM-targeting sequence
132 AKAP1 (1-30), was synthetized by GenScript, opened by *Eco*RI/*Xba*I and inserted N-
133 terminally into the ScGI sequence preceded by a linker $A(EAAAK)^5A$ to separate the fusion
134 proteins and keep the flexibility[16]. The nucleotide sequences for ScGI has been deposited in
135 GenBank under the accession number OP221137. ScGI and OMM-ScGI biosensors were then
136 packaged in adenovirus type 5, amplified and titer measured by VectorBiolabs (Malvern, PA).

137 **Transfection of HEK293 cells and *in vitro* FRET assay.** HEK293 cells were cultured in
138 Dulbecco's modified Eagle's medium (DMEM) with GlutaMAX supplemented with 10% fetal
139 bovine serum (FBS) and 100 U penicillin/streptomycin at 37ºC in a humidified atmosphere of
140 5% CO_2 in air. Cells were transiently transfected with the indicated plasmids using
141 LipofectAMINE 2000 (ThermoFischer) according to the manufacturer's protocol. After
142 transfection, cells were cultured for 48 h, then homogenized with Ultra-Turrax (Franke &
143 Kunkel KG, Staufen, Germany) for 30 s at 4°C in Buffer A (HEPES 10 mM pH 7.3, NaCl 137
144 mM, KCl 5.4 mM, $CaCl_2$ 2 mM, $MgCl_2$ 1 mM). Homogenates were stimulated with increasing
145 concentrations of cGMP or/and cAMP in the presence of IBMX (100 µM). The donor
146 fluorophore CFP was excited at 430 nm (430/24 filter) and the fluorescence emission (F) of
147 Venus and CFP were measured (535/25 and 470/24 nm, respectively) in an EnVision plate
148 reader (PerkinElmer, USA, NY, Melville). Venus emission was corrected for spillover of CFP
149 emission into the Venus channel (72.3%). The FRET response was calculated as changes in
150 F_{Venus}/F_{CFP}. Affinities (pEC_{50}) were calculated by GraphPad Prism 9 for Windows (GraphPad
151 Software, San Diego, CA) where the lowest FRET was set as the highest concentration of
152 cGMP.

153 **Confocal microscopy.** *Evaluation of the FRET biosensors localization at mitochondria:* Rat
154 heart derived H9c2 cardiac myoblasts (Sigma-Aldrich, St.Louis, MO) were cultured in
155 Dulbecco's modified Eagle's medium (DMEM) with GlutaMAX supplemented with 10% fetal
156 bovine serum (FBS), 100 U penicillin/streptomycin, 100 mM sodium pyruvate and 100 mM
157 MEM NEAA at 37ºC in a humidified 5% CO_2–95% air atmosphere. Cells were transiently

158 transfected with the indicated plasmids using LipofectAMINE 2000 (ThermoFisher) according
159 to the manufacturer's protocol and cultured on poly-lysin coated glass cover-slides. Rat adult
160 cardiomyocytes were plated in laminin coated cover-slides and transduced with adenovirus
161 containing the biosensor as previously described[17,18]. After 48 h transfection (H9c2) and
162 transduction (cardiomyocytes), cells were incubated with 50 nM Mitotracker Deep Red
163 (ThermoFisher) for 30 min, washed and incubated in Buffer B (NaCl 144 mM, KCl 1.97 mM,
164 $CaCl_2$ 1 mM, $MgCl_2$ 1 mM, KH_2PO_4 0.43 mM, K_2HPO_4 1.5 mM, glucose 10 mM) to be
165 visualized under an Olympus FV1000/BX61 confocal microscope using a water immersion
166 objective (60x 1.1 NA). Cells were sequentially excited with a 488 nm laser for CFP and a 633
167 nm laser for the Mitotracker Deep Red and the emission was measured by Olympus Fluoview
168 (Olympus, Tokyo, Japan) at 510/25 nm for CFP and 664/20 nm for Mitotracker Deep Red.
169 *Evaluation of mitochondria morphology:* H9c2 cells were cultured on poly-lysin coated glass
170 cover-slides and after 24 h stimulated as indicated and incubated with 50 nM Mitotracker Green
171 for 15 min, washed and incubated in Buffer B. Cells were visualized under an Olympus
172 FV1000/BX61 confocal microscope using a water immersion objective (60x 1.1 NA). Cells
173 were excited with a 488 nm laser and the emission was measured by Olympus Fluoview 1000
174 at 510/25 nm. Images were analysed by Mito-Morphology ImageJ macro[19], which was
175 modified for this measurements to apply a Gaussian filter. In brief, the macro extracts the green
176 channel (stained with Mitotracker Green) to grayscale, inverts to a binary mask and thresholds
177 to resolve mitochondria; these are analysed as particles and different morphology parameters
178 are generated. Among them the ratio between the major and minor axis for each mitochondria
179 was employed as index of mitochondria elongation. For each cell the median of these values
180 was calculated.

181 **FRET imaging**. H9c2 cells and cardiomyocytes expressing the indicated biosensors (as
182 described above) were placed into a watertight cell imaging chamber (Attofluor, ThermoFisher)
183 at room temperature in Buffer B. Cells were visualized through a motorized digital inverted
184 fluorescent microscope (iMIC; FEI, Graefelfing, Germany) with an oil objective (40x, 1.35
185 NA; Olympus). Fluorescent molecules were illuminated by a monochromator with fast-
186 switching wavelengths (Polychrome V; FEI) for 20-80 ms at a frequency of 0.1-1 Hz. Cells
187 were excited at 436±10 nm for 20-80 ms and emission was split using a dichrotome iMIC Dual
188 Emission Module with a DCLP 505 filter that separates the two fluorophores onto a camera
189 (EVOLVE 512; Photometrics, Tucson, USA). Fluorescence was measured at 530±15 nm for
190 Venus and at 470±12 nm for CFP emission. Images were acquired by Live Acquisition browser

191 (FEI) and FRET was calculated using Offline Analysis software (FEI). FRET was measured
192 as F_{Venus}/F_{CFP}. Venus emission was corrected for spillover of CFP emission into the Venus
193 channel (63%). FRET was adjusted for photobleaching. In a subset of experiments, cells were
194 visualized through a motorized digital inverted microscope (IX81; Olympus) with an oil
195 objective (40x, 1.35 NA; Olympus). Fluorescent molecules were excited at 436nm for 8-20ms
196 (CoolLed pE-4000) and emission split with a 495 nm filter using an Optosplit II (Cairn
197 research, Kent, UK) separating two fluorophores onto a camera (Prime 95B; Photometrics).
198 Fluorescence was measured at 535±15 nm for Venus and at 470±12 nm for CFP emission.
199 Images were acquired by Micro-Manager. FRET was measured as F_{Venus}/F_{CFP} through custom-
200 built scripts in ImageJ. Representative experiments were run through a Savitzky–Golay filter
201 using GraphPad Prism 9 for Windows for clarity.

202 **Total cGMP measurements.** H9c2 cells and isolated ventricular cardiomyocytes plated for
203 20h were stimulated with ANP (1μM) or CNP (1μM) for 10 min, 30 min, 1, 3, 6, 12 and 24 h.
204 Cyclic GMP levels were measured using a cGMP enzyme immunoassay kit (Cayman Chemical
205 Company, Ann Arbor, MI, USA) as previously described [20].

206 **Statistics.** Statistical significance was determined by one-way ANOVA with Bonferroni's,
207 Dunett's, Tukey's and Sidak's multiple comparisons test, two-way ANOVA with Sidak's
208 multiple comparisons test as indicated using GraphPad Prism 9 for Windows. $P<0.05$ was
209 considered statistically significant.

210

211 **Results**

212 *Natriuretic peptides increase cell viability*

213 In order to study the effects of NPs on cell survival, we first measured the degree of cell
214 viability of cardiomyocytes cultured for 20 h in a medium deprived of insulin and
215 triiodothyronine (T3) to induce stress to the cells. During cell death, LDH is released to the
216 medium, and this was measured over the next 24 h and progressively showed a time-dependent
217 increase in cell death (Figure 1a). To determine if NPs could modify cell viability, we
218 stimulated cardiomyocytes with CNP (1μM) or ANP (1μM) and found that both natriuretic
219 peptides significantly reduced LDH levels in the medium compared to vehicle over time
220 (Figure 1a). This indicates a protective effect of CNP and ANP against cardiomyocyte death.
221 Further, we assessed the production of ATP as an indicator of metabolically active cells. A 3 h
222 stimulation with CNP or ANP increased ATP levels (CNP:1.6±0.1 and ANP:1.8±0.2 fold
223 increase *vs.* control). In addition, 24 h stimulation with either CNP or ANP also increased ATP
224 levels (CNP:1.4±0.1 and ANP:1.4±0.1 fold *vs.* control; Figure 1b) suggesting that NPs increase
225 cell viability, in line with our results on LDH measurements. To determine whether NPs
226 increase cGMP over such prolonged periods (24h), cardiomyocytes were stimulated with CNP
227 or ANP for up to 24 h and we found that CNP-stimulation increased cGMP over the entire 24
228 h showing peak levels around 1 h, while ANP stimulation increased cGMP with a peak around
229 30 min and gave an earlier decrease in cGMP levels than CNP (Supplementary Fig. 1). These
230 data suggest that cGMP increases are sustained and can mediate downstream effects on cell
231 viability during prolonged NP stimulation.

232

233 *NPs protect against apoptosis through the mitochondrial intrinsic pathway*

234 LDH release from damaged cells could result from either necrosis or apoptosis. We therefore
235 wanted to explore if NPs could alter apoptosis and performed TUNEL assay on adult
236 cardiomyocytes. Stimulating cardiomyocytes for 3 h with either CNP or ANP reduced the
237 number of apoptotic cells (76.1±5.3% and 65.9±8.3% compared to control, respectively; Figure
238 2a). To verify the effects of NPs on apoptosis, we measured the cleavage of PARP, which will
239 prevent PARP from repairing DNA damage and therefore induce apoptosis. Stimulation with
240 CNP or ANP for 3 h significantly decreased PARP cleavage (Figure 2b). Taken together, these
241 data suggest that both CNP and ANP reduce apoptotic cell death.

242 To investigate if the NP-mediated protective effect against apoptosis was through the intrinsic
243 apoptotic pathway, we measured the activation of caspase 9, which depends on cytochrome c
244 release from the mitochondria. CNP- and ANP-stimulation for 3 h significantly reduced the
245 levels of cleaved caspase 9 compared to control (Figure 2c). In addition, CNP and ANP
246 significantly reduced levels of cytochrome c in the cytosol compared to the control (82.7%
247 ±5.3 (CNP) and 76.7% ± 8.3 (ANP) of control, Figure 2d). Together, these data show that both
248 NPs prevent cardiomyocyte apoptosis through the intrinsic mitochondrial pathway.

249

250 *Development of selective FRET-based cGMP biosensors targeted to mitochondria*

251 Since NPs reduced mitochondria-induced apoptosis, we wanted to explore if NPs increased
252 cGMP levels around mitochondria.

253 We have previously shown that cGMP increases in different cellular microdomains by NP-
254 stimulation, using both untargeted and localized FRET-based biosensors in adult
255 cardiomyocytes [21,22] and others have shown that stimulation of soluble guanylyl cyclase (sGC)
256 increases cGMP at the OMM in neonatal cardiomyocytes using an OMM-localized FRET-
257 based biosensor[23]. To investigate whether NPs increase cGMP at the mitochondria, we
258 developed FRET-based cGMP biosensors that measure cGMP in the cytosol and at the outer
259 mitochondrial membrane. We first constructed a potentially brighter variant of the previously
260 published cGi-500 biosensor[24] by replacing the acceptor fluorophore with Venus and termed
261 this new biosensor cGi-500V (Figure 3a). We then expressed the biosensor in HEK293 cells
262 and determined its affinity for cGMP by incubating cell homogenates with increasing
263 concentrations of cGMP. The resulting biosensor had an affinity (EC_{50}) of 510±42 nM (Figure
264 3a) for cGMP with a maximal change in FRET of 53.2±1.4 % (Figure 3d).

265 Cyclic AMP is structurally similar to cGMP and many biosensors only display moderate
266 selectivity between these nucleotides[21,25]. Since cGMP can directly and indirectly modulate
267 cellular concentrations of cAMP through inhibition or activation of certain PDEs[26,27],
268 biosensors with low cyclic nucleotide selectivity can indiscriminately bind either cyclic
269 nucleotides. It is therefore essential to engineer a biosensor with high cGMP selectivity. First
270 we measured FRET of cGi-500V in the presence of cAMP. FRET *increased* by 23.7±2.4 % at
271 low cAMP concentrations (EC_{50High} 12.1±1.8 nM), while FRET decreased at higher
272 concentrations of cAMP (EC_{50Low} 106±28 μM) (Figure 3a and Table 1) demonstrating that
273 cAMP can bind cGi-500V and low level of cAMP can interfere with the FRET responses for

274 cGMP. cGi-500V is based on the tandem cyclic nucleotide binding (CNB) domains of cGMP-
275 dependent protein kinase Iα with different cyclic nucleotide affinities. Only the C-terminal
276 CNB-domain (CNB-B) is selective for cGMP and its co-crystal structure with cGMP showed
277 that an arginine residue at β5 is responsible for the enzyme selectivity[28]. The N-terminal CNB
278 domain (CNB-A) binds both cGMP and cAMP with similarly high affinities with little cyclic
279 nucleotide selectivity. It contains a cysteine at the corresponding position in β5 instead of
280 arginine[28]. We therefore mutated this cysteine (C158) in the CNBD-A to an arginine and
281 termed the mutant biosensor ScGI (Selective cyclic GMP kinase I sensor). Cyclic AMP did not
282 show high affinity increase in FRET (as that obtained with the cGi-500V) and only a reduction
283 of FRET was observed for the higher cAMP concentrations (EC_{50} of 125±23 μM; Figure 3b
284 and Table 1). The ScGI biosensor also displayed a ~ 2 fold *increased* affinity for cGMP
285 (216±18 nM) compared to the cGi-500V resulting in ~500 fold cGMP selectivity over cAMP.
286 However, the mutation caused a reduction in the maximal FRET observed (34.0±3.6% *vs*.
287 53.2±1.4% for the cGi-500V, Figure 3d).

288 Since the ScGI with Cys158Arg no longer responded to the high affinity cAMP binding,
289 and the affinity for cGMP closely matched previously published affinity for the isolated CNB-
290 B[28], we hypothesized that the cGMP-induced FRET change in both cGI-500V and ScGI was
291 only due to binding of cGMP to the CNBD-B. To test this, we determined if the presence of
292 cAMP influenced cGMP-binding to the cGI-500V and ScGI biosensors in an *in vitro*
293 competition-binding assay. Adding a low concentration (1μM) of cAMP increased FRET of
294 the cGI-500V by 25.0±1.7 %, but did not alter the affinity for cGMP (EC_{50} of 321±61 nM;
295 Table 1; Supplementary Fig. 2). Adding a high concentration of cAMP (100μM) slightly
296 reduced FRET (9.2±2.1 % reduction) and significantly decreased the potency of cGMP by ~ 2
297 fold (EC_{50} 1173±202 nM) (Supplementary Fig. 2). For the ScGI biosensor, 1 μM cAMP did
298 not affect the FRET response (7.3±3.6% increase, p=0.08) and did not modify the potency of
299 cGMP (EC_{50} 294±116 nM). Adding 100μM cAMP significantly reduced FRET (37.2±7.3 %
300 reduction) and reduced the cGMP potency by ~ 3 fold (EC_{50} 683±174 nM) (Supplementary Fig.
301 2). Taken together, these data suggest that cAMP at low concentrations binds to the CNBD-A
302 of cGi-500V, which is not responsible for determining the cGMP affinity but rather induces a
303 conformational change of the biosensor and therefore increases FRET. Cyclic AMP at high
304 concentrations, on the other hand, competes with cGMP for binding to the CNB-B in both cGi-
305 500V and ScGI or the Cys158Arg mutation also alters CNB-A affinity for cGMP. In addition,

306 this confirms that the mutation in the CNB-A of the ScGI prevents the high affinity binding of
307 cAMP displayed by the cGi-500V.

308 Next, we constructed a mitochondria-localized ScGI biosensor using the N-terminal
309 targeting sequence of AKAP1, an anchoring protein known to be localized at the OMM and
310 directing PKA signaling[29-31]. This biosensor was termed OMM-ScGI and displayed an affinity
311 for cGMP similar to the untargeted ScGI biosensor (EC_{50} 225.7±32.3 nM) with ~200 fold
312 selectivity *vs*. cAMP (EC_{50} 52±11 μM) (Figure 3c and Table 1). However, adding this tag to
313 the ScGI biosensor decreased the maximal change in FRET significantly compared to the
314 untargeted sensor (14.6±0.4%, Figure 3d).

315

316 *Real time measurement of cGMP around mitochondria*

317 To determine if the OMM-ScGI biosensor displayed mitochondrial targeting, we expressed the
318 ScGI and OMM-ScGI in H9c2 cells and in adult rat ventricular cardiomyocytes and determined
319 if these co-stained with the mitochondrial marker Mitotracker Deep Red. The OMM-ScGI
320 biosensor co-localized with Mitotracker Deep Red while the untargeted biosensor did not
321 (Figure 4a; Supplementary Fig. 3a), suggesting that the OMM-ScGI localizes to the
322 mitochondria. To assess if NPs increased cGMP around this localized biosensor, we stimulated
323 single cells expressing either the ScGI or the OMM-ScGI biosensors with CNP (300 nM)
324 followed by the non-selective PDE inhibitor IBMX (100 μM) to obtain maximal biosensor
325 activation and measured FRET, reflecting cGMP levels (Figure 4b and d; Supplementary Fig.
326 3b and d). Stimulating ScGI-expressing cells with CNP decreased FRET (increase in cGMP)
327 by 90.5±2.0% of max in H9c2 and by 68.8±3.1% of max in cardiomyocytes, while in OMM-
328 ScGI expressing cells, CNP decreased FRET by 81.1±4.3% of maximum in H9c2 and by
329 66.6±4.3% of maximum in cardiomyocytes (Figure 4 b-d; Supplementary Fig. 3b-d). This
330 suggests that GC-B stimulation causes an increase in cGMP in the cytosol, as previously
331 shown[21,22,32] and at the OMM; moreover IBMX gave a further increase in cGMP in both the
332 cytosol and at the OMM, indicating that PDEs regulate these pools of cGMP (Figure 4d;
333 Supplementary Fig. 3d).

334 Considering that both CNP and ANP protected against apoptosis, we also wanted to
335 measure the ANP-stimulated cGMP pool. Stimulation of ScGI-expressing cells with ANP
336 (1μM) gave a FRET response of 2.4±1.5% of maximum in H9c2 and of 2.2±1.3% of max in
337 cardiomyocytes (right panels in Figure 4b and Supplementary Fig. 3b). Further stimulation

338 with IBMX gave a FRET response of 5.1±1.1 % in H9c2 and 29.2±3.8% in cardiomyocytes
339 (Figure 4d and Supplementary Fig. 3d). Stimulation of OMM-ScGI-expressing cells with ANP
340 generated a larger response compared to the untargeted sensor, with 21.1±6.7 % of maximum
341 in H9c2 and 15.2±1% of maximum in cardiomyocytes (right panels in Figure 4c and
342 Supplementary Fig. 3c). IBMX gave a further FRET response of 16.1± 2.4% in H9c2 and
343 39.1±2.9% in cardiomyocytes (Figure 4d and Supplementary Fig. 3d). Both biosensors
344 displayed an ANP-induced cGMP increase significantly lower than that induced by CNP, but
345 ANP at the OMM gave a significantly larger response than in the cytosol in adult
346 cardiomyocytes. These data taken together suggest that CNP induces a greater cGMP pool both
347 in the cytosol and at the OMM, while ANP induces a smaller cGMP pool, which instead is
348 restricted to the OMM in adult cardiomyocytes.

349

350 *NPs modulate Drp1 phosphorylation and prevent mitochondrial fragmentation*

351 Mitochondrial function is modulated by phosphorylation/dephosphorylation of several proteins
352 involved in mitochondrial dynamics. Among these, phosphorylation of Drp1 at Ser637 was
353 found to protect against apoptosis and mitochondrial fragmentation [33-35]. We therefore
354 investigated whether NPs modulate phosphorylation of Drp1 in adult cardiomyocytes and
355 found that both CNP and ANP increased phosphorylation at Ser637, with CNP giving a
356 significantly greater phosphorylation compared to ANP (Figure 5a) without affecting the total
357 protein expression (Supplementary Fig. 4). Therefore we tested whether NPs can prevent
358 mitochondrial fragmentation in H9c2 cells undergoing H_2O_2-mediated apoptosis. Firstly, we
359 measured CNP- and ANP-mediated cGMP increase in H9c2 cells over 24 h and found that
360 cGMP levels reach a peak already at 10 min and with an increase above basal maintained
361 troughout 12 h for CNP and ANP (Supplementary Fig. 5). Therefore, we stimulated H9c2
362 cells with H_2O_2 (100μM) for 3h and showed that mitochondria are significantly fragmented
363 compared to control cells (Figure 5b) and that concomitant CNP stimulation for 3 h
364 significantly inhibited mitochondrial fragmentation induced by H_2O_2 (Figure 5b). ANP, on the
365 other hand, did not modify H_2O_2-induced mitochondrial fragmentation (Figure 5b), even
366 though the proportion of cells with elongated mitochondria was slightly increased (30.4% with
367 H_2O_2 + ANP *vs* 18.5% with H_2O_2; Table 2; not significantly different). All together, these data
368 suggest that NPs prevent cell apoptosis through the instrinsic mitochondrial pathway, possibly
369 involving Drp1 phosphorylation and reduced mitochondrial fragmentation.

370 **Discussion**

371 In this study, we show that the natriuretic peptides CNP and ANP protect against apoptosis of
372 cardiomyocytes, with reduced PARP cleavage and increase in cell viability. Moreover, we
373 show that the natriuretic peptides reduce both activation of caspase 9 and release of cytochrome
374 c from mitochondria to the cytosol, suggesting that the protective effects involve the
375 mitochondrial intrinsic pathway. Further, by constructing a selective biosensor and targeting
376 this to the OMM, we also show that ANP and CNP increase cGMP at the outer mitochondrial
377 membrane in cardiomyocytes. In addition, both CNP and ANP increase Drp1 phosphorylation,
378 with CNP also preventing mitochondrial fragmentation, likely protecting mitochondria from
379 apoptosis.

380

381 *Natriuretic peptide effects on apoptosis*

382 Here we demonstrate increased survival of adult cardiomyocytes and protection from apoptosis
383 by NP stimulation. Previous studies determining the effects of NPs on regulation of apoptosis
384 show conflicting results: some studies found that stimulating GC-A and/or GC-B is protective
385 against apoptosis, mostly in other cell types[36-39], but also in cardiomyocytes and the heart[40,41].
386 However, these studies used neonatal cardiomyocytes, which have a lower degree of
387 differentiation, and focussed on ANP signalling specifically at the nuclei. Others showed an
388 increase in apoptosis by NPs in cardiomyocytes[42-45] and in other tissues[46]. However, the
389 different results between the studies showing increased apoptosis and the data presented in this
390 study could potentially be due to study of adult (this study) *vs*. neonatal cardiomyocytes[42,44,45]
391 or normal (this study) *vs*. a heart failure model[43].

392

393 *NPs/cGMP signalling involved in mitochondrial function*

394 Our results show that ANP and CNP increase cGMP at the OMM. Cyclic GMP has previously
395 been found in cardiac mitochondria, where mtNOS and sGC have been reported to be located
396 in the matrix[47-49] and sGC-generated cGMP has also been found at the OMM [23]. However,
397 those studies did not examine natriuretic peptide signalling.

398 The exact mechanism of how NPs regulate mitochondrial function and prevent apoptosis
399 remains elusive. Some studies show that NPs promote mitochondrial biogenesis by
400 upregulation of PGC-1α and PPARδ that could protect cardiomyocytes against mitochondria-

401 mediated apoptosis[50,51]. Moreover, PKG I seems to protect against apoptosis by increasing
402 expression of Bcl-2 and decreasing Bax in adult rat cardiomyocytes subjected to
403 ischemia/reoxygenation stress[52]. Further, ANP- and BNP-stimulation has been shown to induce
404 mitoK_{ATP} opening and prevent mitochondrial permeability transition pore opening, where both
405 mechanisms are protective against apoptosis[41,53-55]. A third pathway for NP regulation of
406 mitochondrial function could be through regulation of Drp1. It has earlier been shown that
407 PKA can phosphorylate Drp1 at S637, reducing its activity [33], and this has been associated with
408 prevention of apoptosis [34,35]. PKG-mediated phosphorylation of Drp1 and its protective effect
409 has been shown via the NO/cGMP pathway in myogenic precursor cells [56]. Thus, there are
410 several possible pathways for how natriuretic peptides can regulate apoptosis, involving either
411 gene regulation or direct regulation of apoptotic pathways. In the present study, we show that
412 NPs increase phosphorylation of Drp1 at Ser637. This could prevent Drp1 activation and
413 initiation of mitochondrial fragmentation, as shown by CNP stimulation (Figure 5b), and thus
414 possibly cause prevention of apoptosis[57]. However, we cannot rule out that other pathways are
415 also involved. Our results show comparable effects of CNP and ANP on LDH activity in the
416 medium, ATP production, PARP cleavage, cleaved caspase 9 and cytochrome c release in
417 addition to the prevention of apoptosis. However, compared to CNP, ANP gave significantly
418 lower cGMP levels at the OMM and also lower Drp1 phosphorylation that did not translate
419 into reduced H_2O_2-induced mitochondrial fragmentation. This might indicate that different
420 pathways are involved in the anti-apoptotic effects seen after ANP and CNP stimulation.
421 Alternatively, the magnitude of Drp1 phosphorylation seen after ANP stimulation is sufficient
422 to inhibit the mitochondrial intrinsic pathway.

423

424 *FRET-based biosensors detect cGMP increase at the mitochondrial outer membrane*

425 The larger phosphorylation of Drp1 and reduced mitochondria fragmentation by CNP,
426 compared to ANP is in line with the differential cGMP levels measured by FRET biosensor at
427 the OMM (Figure 4 and 5). There are some indications for the presence and effect of cGMP
428 inside the mitochondrial matrix and at the OMM after stimulation of sGC[23,41,47-49,53-55].
429 However, the role of NP-stimulated cGMP at the OMM shown herein has not been examined
430 previously. More is known about the role of cAMP in the mitochondria, which was found both
431 in the matrix[58,59] and at the OMM, where PKA and PDE2A activity were also present [35,60]. In
432 these studies a mitochondrial-localized FRET-based biosensor for cAMP was used[35,59], and
433 recently also a FRET-based biosensor for cGMP localized at the OMM was developed [23].

434 However, that biosensor used the cGi-500 biosensor which did not show high selectivity *vs.*
435 cAMP in our hands (Figure 3; Table 1). Therefore, we constructed cGMP-selective biosensors
436 localized to the OMM to investigate the presence of cGMP around mitochondria.

437 Several FRET-based biosensors have been developed with different fluorescent
438 proteins, cGMP binding domains and affinity/selectivity profiles. Among the most sensitive
439 biosensors, we find the red-cGES-DE5, Yellow *Pf*PKG and Red *Pf*PKG biosensors[21,32], with
440 cGMP affinity in the nM range, and the cGi-500 biosensor[24], which is >10 times less sensitive.
441 The untargeted ScGI and the OMM-ScGI biosensors constructed in this study presented a mid-
442 range affinity with an EC_{50} of around 200 nM, and were shown to be sensitive enough to detect
443 similar increases of cGMP by CNP stimulation compared to the other biosensors (Figure 4d,
444 Supplementary Fig. 3d). ANP stimulation, however, gave a significant increase in cGMP only
445 at the OMM and not with the untargeted biosensor in cardiomyocytes (Figure 4d), indicating
446 that GC-A stimulation locally increases cGMP around the OMM. CNP has previously been
447 shown to stimulate GC-B both in the crest and T-tubules and produce cGMP that reaches
448 remote targets in cardiomyocytes [22,61], therefore the cGMP increase at the OMM could reflect
449 the widespread CNP-induced cGMP increase. ANP, on the other hand, has been reported to
450 produce a small cGMP pool confined near the plasma membrane by activation of GC-A only
451 in the T-tubules of cardiomyocytes [61]. Such local cGMP increase might not be detected by an
452 untargeted biosensor due to widespread distribution and local signals being "diluted" across
453 the entire cell. In fact, even using the ~10 times more sensitive untargeted Yellow *Pf*PKG
454 biosensor we could only detect a modest cGMP increase after GC-A stimulation[21]. Since ANP
455 increases cGMP considerably more at the OMM nanodomain compared to that detected by the
456 untargeted biosensors in cardiomyocytes (Figure 4d), the GC-A receptor and therefore its
457 cGMP pool at the T-tubules might be in close vicinity of the OMM and form a nanodomain.
458 Given that mitochondria are tightly distributed between the sarcomeres but also in the sub-
459 sarcolemmal region[62], either the membranal localization of the GCs or the different ability of
460 cGMP from the GC-A and GC-B to reach different targets, could help explain the higher levels
461 of cGMP detected in the OMM by CNP compared to ANP.

462 CNB domains *responsible for inducing changes in FRET in the cGI biosensors*

463 Given that cAMP is structurally similar to cGMP and that basal cAMP concentration in
464 cardiomyocytes are higher (1μM) than cGMP (10nM)[32,63,64], it is important to determine the
465 selectivity of cGMP biosensors and to ensure that the response is representative of increases in
466 cGMP and not cAMP. In our hands, the cGi-500V showed a poor selectivity profile, where

467 cAMP bound to the biosensor at low concentrations resulting in *increased* FRET (Figure 3a).
468 However, these concentrations of cAMP did not compete with the ability of cGMP to alter
469 FRET (Supplementary Fig. 2a). In addition, when mutating the CNB-A domain (in the ScGI),
470 the increase in FRET by low cAMP concentrations was prevented, whereas the cGMP potency
471 was only slightly *increased* (Figure 3b and Supplementary Fig. 2b). It has previously been
472 shown that the CNB-A domain displays similar high affinity for both cGMP and cAMP[65],
473 whereas the CNB-B domain has a slightly lower affinity for cGMP (~215nM), but the affinity
474 for cAMP is much lower (EC_{50}=52µM) and the CNB-B domain is therefore responsible for the
475 cGMP selectivity of PKG I[28]. Considering that the ScGI has similar affinity for cGMP as the
476 isolated CNB-B domain, this domain could also be solely responsible for the biosensors
477 sensitivity or both CNB domains are responsible, but the response is indistinguishable as both
478 domains now binds cGMP with similar affinity. Taken together, this indicates that 1) the FRET
479 increase seen with low concentrations of cAMP (in the cGi-500V) is possibly due to non-
480 selective cAMP binding to the CNB-A domain, 2) cAMP at high concentrations binds to the
481 CNB-B domain of cGi-500V and ScGI that reduces FRET, and 3) either cGMP binding to the
482 CNB-A does not alter the conformation of PKG to trigger a change in FRET, or cGMP binds
483 to both the CNB-A and –B domains with similar affinity to trigger an increase in the distance
484 between the CFP and Venus, thus reducing FRET. The ScGI biosensor will thus be a valuable
485 tool for determining cGMP, particularly in complex biological systems where cAMP can act
486 as a confounding factor.

487

488 ## Conclusion

489 In conclusion, we present evidence for a protective effect of natriuretic peptides against
490 cardiomyocyte apoptosis, mediated by the intrinsic apoptotic pathway, which also involves
491 phosphorylation of Drp1 and reduced mitochondrial fragmentation. Further, we constructed a
492 novel FRET-based biosensor with high cGMP selectivity in order to detect cGMP at the
493 mitochondria and show that both CNP and ANP increase cGMP at the OMM.

494

495 ## Acknowledgements

496 The authors wish to thank Iwona Gutowska Schiander (University of Oslo) and Soheil Naderi
497 (Oslo University Hospital) for excellent technical assistance.

Funding

This work was supported by the South-Eastern Norway Regional Health Authority (grant # 2015036 and 2019051), the Norwegian Council on Cardiovascular Diseases, The Research Council of Norway (grant # 205167 and 303490), The Anders Jahre Foundation for the Promotion of Science, The Family Blix Foundation, The Simon Fougner Hartmann Family Foundation, and grants from the University of Oslo

Ethics declarations

The authors declare no competing interests.

Author Contribution

GC, BDN, CK, KWA and LRM designed research; GC, BDN, DA and MO performed research. GC, BDN, DA, MO, FOL, KWA and LRM analyzed data; GC, KWA and LRM wrote the manuscript. All authors revised and approved the manuscript.

Data availability

Nucleotide sequence for ScGI and OMM-ScGI have been deposited in GenBank. The data that support the findings of this study are available from the corresponding author upon request. The authors declare that the data supporting the findings of this study are available within the paper and its supplementary information files.

516 ## References

517 1 Munzel, T. *et al.* Impact of Oxidative Stress on the Heart and Vasculature: Part 2 of a 3-Part
518 Series. *J. Am. Coll. Cardiol.* **70**, 212-229, doi:10.1016/j.jacc.2017.05.035 (2017).
519 2 Stanley, W. C., Recchia, F. A. & Lopaschuk, G. D. Myocardial Substrate Metabolism in the
520 Normal and Failing Heart. *Physiol. Rev.* **85**, 1093-1129, doi:10.1152/physrev.00006.2004
521 (2005).
522 3 Bertero, E. & Maack, C. Metabolic remodelling in heart failure. *Nat. Rev. Cardiol.* **15**, 457-470,
523 doi:10.1038/s41569-018-0044-6 (2018).
524 4 Braschi, E. & McBride, H. M. Mitochondria and the culture of the Borg: understanding the
525 integration of mitochondrial function within the reticulum, the cell, and the organism. *Bioessays*
526 **32**, 958-966, doi:10.1002/bies.201000073 (2010).
527 5 Kasahara, A. & Scorrano, L. Mitochondria: from cell death executioners to regulators of cell
528 differentiation. *Trends Cell Biol.* **24**, 761-770, doi:10.1016/j.tcb.2014.08.005 (2014).
529 6 Lee, K. H. *et al.* Cardioprotective effects of PKG activation by soluble GC activator, BAY 60-
530 2770, in ischemia-reperfusion-injured rat hearts. *PLoS One* **12**, e0180207,
531 doi:10.1371/journal.pone.0180207 (2017).
532 7 Frankenreiter, S. *et al.* cGMP-Elevating Compounds and Ischemic Conditioning Provide
533 Cardioprotection Against Ischemia and Reperfusion Injury via Cardiomyocyte-Specific BK
534 Channels. *Circulation* **136**, 2337-2355, doi:doi:10.1161/CIRCULATIONAHA.117.028723
535 (2017).
536 8 Bork, N. I. *et al.* Rise of cGMP by partial phosphodiesterase-3A degradation enhances
537 cardioprotection during hypoxia. *Redox Biology* **48**, 102179,
538 doi:https://doi.org/10.1016/j.redox.2021.102179 (2021).
539 9 Behmenburg, F. *et al.* Impact of Mitochondrial Ca2+-Sensitive Potassium (mBKCa) Channels
540 in Sildenafil-Induced Cardioprotection in Rats. *PLoS One* **10**, e0144737,
541 doi:10.1371/journal.pone.0144737 (2015).
542 10 Frankenreiter, S. *et al.* Cardioprotection by ischemic postconditioning and cGMP-elevating
543 agents involves cardiomyocyte nitric oxide-sensitive guanylyl cyclase. *Cardiovasc. Res.* (2018).
544 11 Volpe, M., Rubattu, S. & Burnett, J., Jr. Natriuretic peptides in cardiovascular diseases: current
545 use and perspectives. *Eur. Heart J.* **35**, 419-425, doi:10.1093/eurheartj/eht466 (2014).
546 12 McMurray, J. J. *et al.* Angiotensin-neprilysin inhibition versus enalapril in heart failure. *N. Engl.*
547 *J. Med.* **371**, 993-1004, doi:10.1056/NEJMoa1409077 (2014).
548 13 Miyashita, K. *et al.* Natriuretic Peptides/cGMP/cGMP-Dependent Protein Kinase Cascades
549 Promote Muscle Mitochondrial Biogenesis and Prevent Obesity. *Diabetes* **58**, 2880-2892,
550 doi:10.2337/db09-0393 (2009).

551 14 Kilkenny, C., Browne, W. J., Cuthill, I. C., Emerson, M. & Altman, D. G. Improving bioscience
552 research reporting: the ARRIVE guidelines for reporting animal research. *PLoS Biol.* **8**,
553 e1000412, doi:10.1371/journal.pbio.1000412 (2010).
554 15 Moltzau, L. R. *et al.* Different Compartmentation of Responses to Brain Natriuretic Peptide
555 and C-Type Natriuretic Peptide in Failing Rat Ventricle. *J. Pharmacol. Exp. Ther.* **350**, 681-
556 690, doi:10.1124/jpet.114.214882 (2014).
557 16 Arai, R., Ueda, H., Kitayama, A., Kamiya, N. & Nagamune, T. Design of the linkers which
558 effectively separate domains of a bifunctional fusion protein. *Protein Eng.* **14**, 529-532 (2001).
559 17 Meier, S. *et al.* PDE3 inhibition by C-type natriuretic peptide-induced cGMP enhances cAMP-
560 mediated signaling in both non-failing and failing hearts. *Eur. J. Pharmacol.* **812**, 174-183,
561 doi:10.1016/j.ejphar.2017.07.014 (2017).
562 18 Orstavik, O. *et al.* The inotropic effect of the active metabolite of levosimendan, OR-1896, is
563 mediated through inhibition of PDE3 in rat ventricular myocardium. *PLoS One* **10**, e0115547,
564 doi:10.1371/journal.pone.0115547 (2015).
565 19 Dagda, R. K. *et al.* Loss of PINK1 function promotes mitophagy through effects on oxidative
566 stress and mitochondrial fission. *J. Biol. Chem.* **284**, 13843-13855,
567 doi:10.1074/jbc.M808515200 (2009).
568 20 Moltzau, L. R. *et al.* SERCA2 activity is involved in the CNP-mediated functional responses
569 in failing rat myocardium. *Br. J. Pharmacol.* **170**, 366-379, doi:10.1111/bph.12282 (2013).
570 21 Calamera, G. *et al.* FRET-based cyclic GMP biosensors measure low cGMP concentrations in
571 cardiomyocytes and neurons. *Commun Biol* **2**, 394, doi:10.1038/s42003-019-0641-x (2019).
572 22 Manfra, O. *et al.* CNP regulates cardiac contractility and increases cGMP near both SERCA
573 and TnI - difference from BNP visualized by targeted cGMP biosensors. *Cardiovasc. Res.*,
574 doi:10.1093/cvr/cvab167 (2021).
575 23 Brescia, M., Chao, Y. C., Koschinski, A., Tomek, J. & Zaccolo, M. Multi-Compartment, Early
576 Disruption of cGMP and cAMP Signalling in Cardiac Myocytes from the mdx Model of
577 Duchenne Muscular Dystrophy. *Int J Mol Sci* **21**, doi:10.3390/ijms21197056 (2020).
578 24 Russwurm, M. *et al.* Design of fluorescence resonance energy transfer (FRET)-based cGMP
579 indicators: a systematic approach. *Biochem. J.* **407**, 69-77, doi:10.1042/BJ20070348 (2007).
580 25 Russwurm, M. & Koesling, D. Measurement of cGMP-generating and -degrading activities and
581 cGMP levels in cells and tissues: Focus on FRET-based cGMP indicators. *Nitric Oxide* **77**, 44-
582 52, doi:10.1016/j.niox.2018.04.006 (2018).
583 26 Omori, K. & Kotera, J. Overview of PDEs and their regulation. *Circ. Res.* **100**, 309-327,
584 doi:10.1161/01.RES.0000256354.95791.f1 (2007).
585 27 Rascon, A. *et al.* Purification and properties of the cGMP-inhibited cAMP phosphodiesterase
586 from bovine aortic smooth muscle. *Biochim. Biophys. Acta* **1134**, 149-156, doi:10.1016/0167-
587 4889(92)90038-d (1992).

588 28 Huang, G. Y. *et al.* Structural basis for cyclic-nucleotide selectivity and cGMP-selective
589 activation of PKG I. *Structure* **22**, 116-124, doi:10.1016/j.str.2013.09.021 (2014).
590 29 Huang, L. J. *et al.* NH2-Terminal targeting motifs direct dual specificity A-kinase-anchoring
591 protein 1 (D-AKAP1) to either mitochondria or endoplasmic reticulum. *J. Cell Biol.* **145**, 951-
592 959, doi:10.1083/jcb.145.5.951 (1999).
593 30 Kim, H. *et al.* Fine-tuning of Drp1/Fis1 availability by AKAP121/Siah2 regulates
594 mitochondrial adaptation to hypoxia. *Mol. Cell* **44**, 532-544 (2011).
595 31 Merrill, R. A. *et al.* Mechanism of Neuroprotective Mitochondrial Remodeling by
596 PKA/AKAP1. *PLoS Biol.* **9**, e1000612, doi:10.1371/journal.pbio.1000612 (2011).
597 32 Götz, K. R. *et al.* Transgenic mice for real-time visualization of cGMP in intact adult
598 cardiomyocytes. *Circ. Res.* **114**, 1235-1245, doi:10.1161/CIRCRESAHA.114.302437 (2014).
599 33 Chang, C.-R. & Blackstone, C. Cyclic AMP-dependent Protein Kinase Phosphorylation of
600 Drp1 Regulates Its GTPase Activity and Mitochondrial Morphology. *J. Biol. Chem.* **282**,
601 21583-21587, doi:10.1074/jbc.C700083200 (2007).
602 34 Cribbs, J. T. & Strack, S. Reversible phosphorylation of Drp1 by cyclic AMP-dependent protein
603 kinase and calcineurin regulates mitochondrial fission and cell death. *EMBO Rep* **8**, 939-944,
604 doi:10.1038/sj.embor.7401062 (2007).
605 35 Monterisi, S. *et al.* PDE2A2 regulates mitochondria morphology and apoptotic cell death via
606 local modulation of cAMP/PKA signalling. *Elife* **6**, doi:10.7554/eLife.21374 (2017).
607 36 Fiscus, R. R., Tu, A. W. & Chew, S. B. C. Natriuretic peptides inhibit apoptosis and prolong
608 the survival of serum-deprived PC12 cells. *Neuroreport* **12**, 185-189 (2001).
609 37 Fiscus, R. R. Involvement of cyclic GMP and protein kinase G in the regulation of apoptosis
610 and survival in neural cells. *Neurosignals* **11**, 175-190 (2002).
611 38 Jin, X., Zhang, Y., Li, X., Zhang, J. & Xu, D. C-type natriuretic peptide ameliorates
612 ischemia/reperfusion-induced acute kidney injury by inhibiting apoptosis and oxidative stress
613 in rats. *Life Sci.* **117**, 40-45 (2014).
614 39 Kulhanek-Heinze, S., Gerbes, A. L., Gerwig, T., Vollmar, A. M. & Kiemer, A. K. Protein
615 kinase A dependent signalling mediates anti-apoptotic effects of the atrial natriuretic peptide in
616 ischemic livers. *J. Hepatol.* **41**, 414-420 (2004).
617 40 Kato, T. *et al.* Atrial natriuretic peptide promotes cardiomyocyte survival by cGMP-dependent
618 nuclear accumulation of zyxin and Akt. *The Journal of clinical investigation* **115**, 2716-2730
619 (2005).
620 41 Sun, Y., Zhang, Y., Yan, M., Wu, Y. & Zheng, X. B-type natriuretic peptide-induced
621 cardioprotection against reperfusion is associated with attenuation of mitochondrial
622 permeability transition. *Biol. Pharm. Bull.* **32**, 1545-1551 (2009).

623 42 Wang, T.-N., Ge, Y.-K., Li, J.-Y., Zeng, X.-H. & Zheng, X.-X. B-type natriuretic peptide
624 enhances mild hypoxia-induced apoptotic cell death in cardiomyocytes. *Biol. Pharm. Bull.* **30**,
625 1084-1090 (2007).
626 43 Qvigstad, E. *et al.* Natriuretic peptides increase beta1-adrenoceptor signalling in failing hearts
627 through phosphodiesterase 3 inhibition. *Cardiovasc. Res.* **85**, 763-772, doi:10.1093/cvr/cvp364
628 (2010).
629 44 Han, B. *et al.* The opposing effects of endothelin-1 and C-type natriuretic peptide on apoptosis
630 of neonatal rat cardiac myocytes. *Eur. J. Pharmacol.* **474**, 15-20 (2003).
631 45 Wu, C.-F., Bishopric, N. H. & Pratt, R. E. Atrial Natriuretic Peptide Induces Apoptosis in
632 Neonatal Rat Cardiac Myocytes. *J. Biol. Chem.* **272**, 14860-14866 (1997).
633 46 Suenobu, N., Shichiri, M., Iwashina, M., Marumo, F. & Hirata, Y. Natriuretic peptides and
634 nitric oxide induce endothelial apoptosis via a cGMP–dependent mechanism. *Arterioscler.*
635 *Thromb. Vasc. Biol.* **19**, 140-146 (1999).
636 47 Costa, L. E. *et al.* Long-term angiotensin II inhibition increases mitochondrial nitric oxide
637 synthase and not antioxidant enzyme activities in rat heart. *J. Hypertens.* **20**, 2487-2494 (2002).
638 48 Boveris, A., D'Amico, G., Lores-Arnaiz, S. & Costa, L. E. Enalapril increases mitochondrial
639 nitric oxide synthase activity in heart and liver. *Antioxidants and Redox Signaling* **5**, 691-697
640 (2003).
641 49 Pozdniakova, S. *et al.* 17β-Estradiol reduces mitochondrial cAMP content and cytochrome
642 oxidase activity in a phosphodiesterase 2-dependent manner. *Br. J. Pharmacol.* **175**, 3876-3890
643 (2018).
644 50 Mitsuishi, M., Miyashita, K. & Itoh, H. cGMP rescues mitochondrial dysfunction induced by
645 glucose and insulin in myocytes. *Biochem. Biophys. Res. Commun.* **367**, 840-845,
646 doi:https://doi.org/10.1016/j.bbrc.2008.01.017 (2008).
647 51 Engeli, S. *et al.* Natriuretic peptides enhance the oxidative capacity of human skeletal muscle.
648 *The Journal of clinical investigation* **122**, 4675-4679 (2012).
649 52 Das, A., Smolenski, A., Lohmann, S. M. & Kukreja, R. C. Cyclic GMP-dependent protein
650 kinase Iα attenuates necrosis and apoptosis following ischemia/reoxygenation in adult
651 cardiomyocyte. *J. Biol. Chem.* **281**, 38644-38652 (2006).
652 53 D'Souza, S. P. *et al.* B-type natriuretic peptide limits infarct size in rat isolated hearts via KATP
653 channel opening. *American Journal of Physiology-Heart and Circulatory Physiology* **284**,
654 H1592-H1600, doi:10.1152/ajpheart.00902.2002 (2003).
655 54 Yang, X.-M., Philipp, S., Downey, J. M. & Cohen, M. V. Atrial natriuretic peptide administered
656 just prior to reperfusion limits infarction in rabbit hearts. **101**, 311-318, doi:10.1007/s00395-
657 006-0587-2 (2006).

658 55 Hong, L. *et al.* Atrial natriuretic peptide prevents the mitochondrial permeability transition pore
659 opening by inactivating glycogen synthase kinase 3β via PKG and PI3K in cardiac H9c2 cells.
660 *Eur. J. Pharmacol.* **695**, 13-19, doi:https://doi.org/10.1016/j.ejphar.2012.07.053 (2012).
661 56 De Palma, C. *et al.* Nitric oxide inhibition of Drp1-mediated mitochondrial fission is critical
662 for myogenic differentiation. *Cell Death Differ.* **17**, 1684-1696, doi:10.1038/cdd.2010.48
663 (2010).
664 57 Hu, C., Huang, Y. & Li, L. Drp1-Dependent Mitochondrial Fission Plays Critical Roles in
665 Physiological and Pathological Progresses in Mammals. *International Journal of Molecular*
666 *Sciences* **18**, 144 (2017).
667 58 Acin-Perez, R. *et al.* Cyclic AMP produced inside mitochondria regulates oxidative
668 phosphorylation. *Cell Metab* **9**, 265-276, doi:10.1016/j.cmet.2009.01.012 (2009).
669 59 DiPilato, L. M., Cheng, X. & Zhang, J. Fluorescent indicators of cAMP and Epac activation
670 reveal differential dynamics of cAMP signaling within discrete subcellular compartments. *Proc.*
671 *Natl. Acad. Sci. U. S. A.* **101**, 16513, doi:10.1073/pnas.0405973101 (2004).
672 60 Lefkimmiatis, K., Leronni, D. & Hofer, A. M. The inner and outer compartments of
673 mitochondria are sites of distinct cAMP/PKA signaling dynamics. *J. Cell Biol.* **202**, 453-462,
674 doi:10.1083/jcb.201303159 (2013).
675 61 Subramanian, H. *et al.* Distinct submembrane localisation compartmentalises cardiac NPR1
676 and NPR2 signalling to cGMP. *Nat Commun* **9**, 2446, doi:10.1038/s41467-018-04891-5 (2018).
677 62 Piquereau, J. *et al.* Mitochondrial dynamics in the adult cardiomyocytes: which roles for a
678 highly specialized cell? *Front. Physiol.* **4**, 102, doi:10.3389/fphys.2013.00102 (2013).
679 63 Sprenger, J. U. *et al.* In vivo model with targeted cAMP biosensor reveals changes in receptor-
680 microdomain communication in cardiac disease. *Nat Commun* **6**, 6965,
681 doi:10.1038/ncomms7965 (2015).
682 64 Koschinski, A. & Zaccolo, M. Activation of PKA in cell requires higher concentration of cAMP
683 than in vitro: implications for compartmentalization of cAMP signalling. *Sci. Rep.* **7**, 14090,
684 doi:10.1038/s41598-017-13021-y (2017).
685 65 Kim, J. J. *et al.* Co-Crystal Structures of PKG Iβ (92–227) with cGMP and cAMP Reveal the
686 Molecular Details of Cyclic-Nucleotide Binding. *PLoS One* **6**, e18413,
687 doi:10.1371/journal.pone.0018413 (2011).

688

689

690

691

692 **Tables**

693 **Table 1.**

694 **Sensitivity and dynamic range of the FRET biosensors.**

695 HEK293 cells expressing the indicated biosensor were homogenized and incubated with
696 increasing concentration of cGMP or cAMP (where indicated) and fluorescence measured as
697 described in Materials and Methods. The maximal FRET change was determined at the highest
698 cGMP concentrations. EC_{50} values shown in µM were calculated from the average pEC_{50}
699 values. Results shown are mean±SEM of 5-12 experiments. *p<0.001 and †p<0.0001 *vs*. cGi-
700 500V; ‡p<0.01 for cGMP EC_{50} *vs*. cGMP EC_{50} +100µM cAMP (One-way ANOVA, with
701 Sidak's post hoc test).

702

	cGMP		**cAMP**		**cAMP**		**cGMP +1µM cAMP**		**cGMP +100µM cAMP**		**Max FRET change (%)**
Sensor	pEC_{50}	EC_{50} (µM)	pEC_{50High}	EC_{50} (µM)	pEC_{50Low}	EC_{50} (µM)	pEC_{50}	EC_{50} (µM)	pEC_{50}	EC_{50} (µM)	
cGi-500V	6.31±0.04	0.5	7.93±0.06	12	4.04±0.13	106	6.52±0.08	0.3	5.94±0.06‡	1.1	53.24±1.43
ScGI	6.68±0.03*	0.2			3.97±0.03	125	6.65±0.16	0.2	6.24±0.14‡	0.6	34.08±3.62†
OMM-ScGI	6.66±0.06*	0.2			4.32±0.12	52					14.62±0.41†

703

704

705

706

707

708

709

710

711

712

713 **Table 2.**

714 **Fraction of fragmented *vs.* elongated mitochondria.**

715 Data from Figure 5 were distributed in two different fractions per each group, where cells
716 with mitochondrial elongation (axis ratio) smaller than 1.75 were considered as having
717 fragmented mitochondria and cells with mitochondria larger than 1.75 were considered as
718 having elongated mitochondria. The threshold was chosen based on mitochondria size
719 distribution in Ctr group. Fractions are indicated as per cent of total number of cells per each
720 group.

721

Mitochondrial elongation	**Ctr**	**CNP**	**ANP**	**H_2O_2**	**H_2O_2+CNP**	**H_2O_2 +ANP**
<1.75 (fragmented)	30.9%	16.8%	38.8%	81.5%	56.9%	69.6%
>1.75 (elongated)	69.1%	83.2%	61.2%	18.5%	43.1%	30.4%

722

723 **Figures**

Figure 1

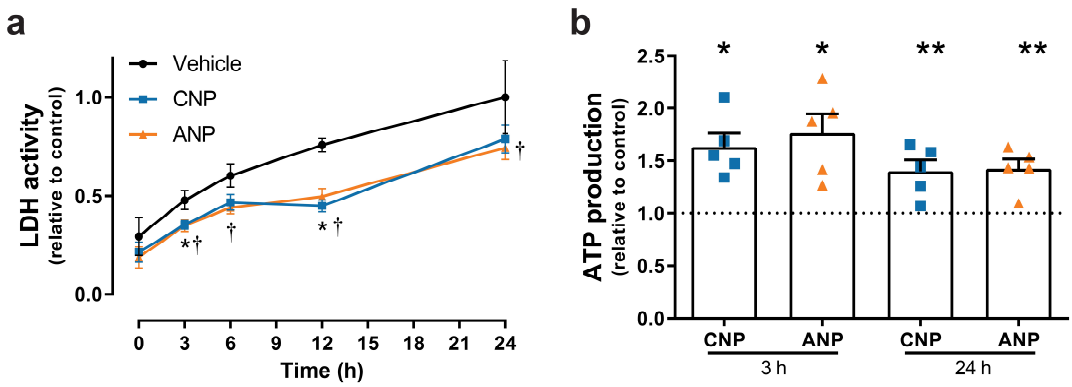

724

725 **Figure 1. NPs reduce cell death and increase ATP levels compared to the control. a)**
726 Cardiomyocytes were stimulated with Vehicle (H_2O), CNP (1µM) or ANP (1µM) for 24 h and
727 sampling of the medium performed at the indicated time. LDH activity in the medium was
728 determined as described in Materials and Methods. LDH activity at 24 h from Vehicle was
729 used as control. Data shown are mean±SEM of 8 independent experiments. *p <0.05 compared
730 to vehicle (two-way ANOVA with Dunnett's multiple comparisons test). **b)** Cardiomyocytes
731 were stimulated with vehicle (control), CNP (1µM) or ANP (1µM) for the indicated times and
732 ATP levels measured as described in Materials and Methods and normalized to control
733 (44±14x10^3 RLU/µg protein at 3h and 26±10x10^3 RLU/µg protein at 24h). Data shown are
734 mean±SEM of 5 independent experiments. *p<0.05 and **p<0.01 compared to control (one-
735 way ANOVA with Sidak's test).

Figure 2

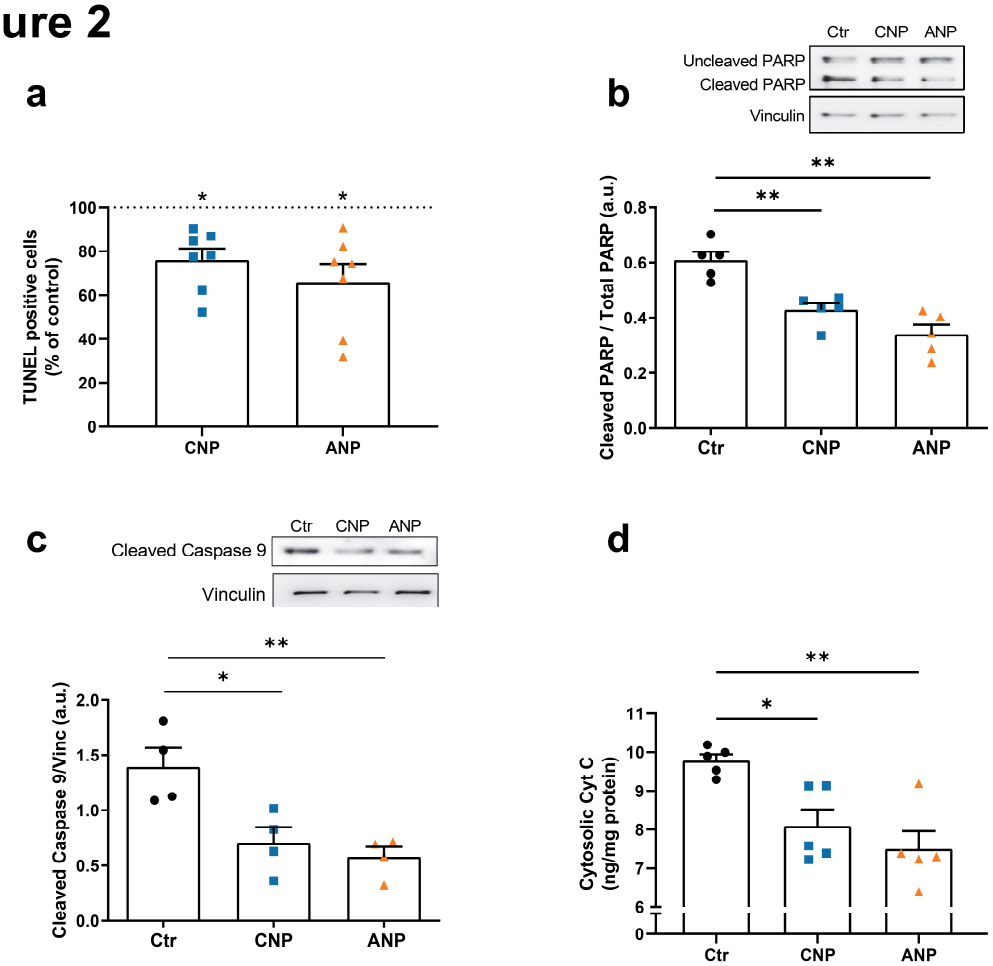

Figure 2. NPs protect against apoptosis through the mitochondrial intrinsic pathway. Cardiomyocytes were incubated with vehicle (H_2O, control), CNP (1µM) or ANP (1µM) for 3 h. **a)** Cells were fixed in 1% paraformaldehyde and fragmented DNA was stained by anti-digoxigenin antibody conjugated with fluorescein. Total number of cells and TUNEL positive cells were counted and shown as a per cent of vehicle treated cells (29.4 % ±3.2). Data shown are mean±SEM of 7 independent experiments. **b)** Cells were lysed and the amount of uncleaved and cleaved PARP and vinculin (loading control) were determined as described in Materials and Methods. Insert shows a representative blot. Data are mean±SEM of 5 independent experiments. **c)** Cells were lysed and active caspase 9 was determined as described in Materials and Methods and normalized to vinculin. Insert shows a representative blot. Quantification of cleaved caspase 9 as a fraction of the loading control (vinculin) and are shown as mean±SEM of 4 independent experiments. **d)** Cytochrome c levels were measured in the cytosolic fraction as described in Material and Methods. Values shown are mean±SEM of 5 independent experiments. *$p<0.05$ and **$p<0.01$ *vs*. Ctr (one-way ANOVA with Sidak's (**a**) or Dunnett's multiple comparisons (**b-d**) test. a.u.: Arbitrary units.

Figure 3

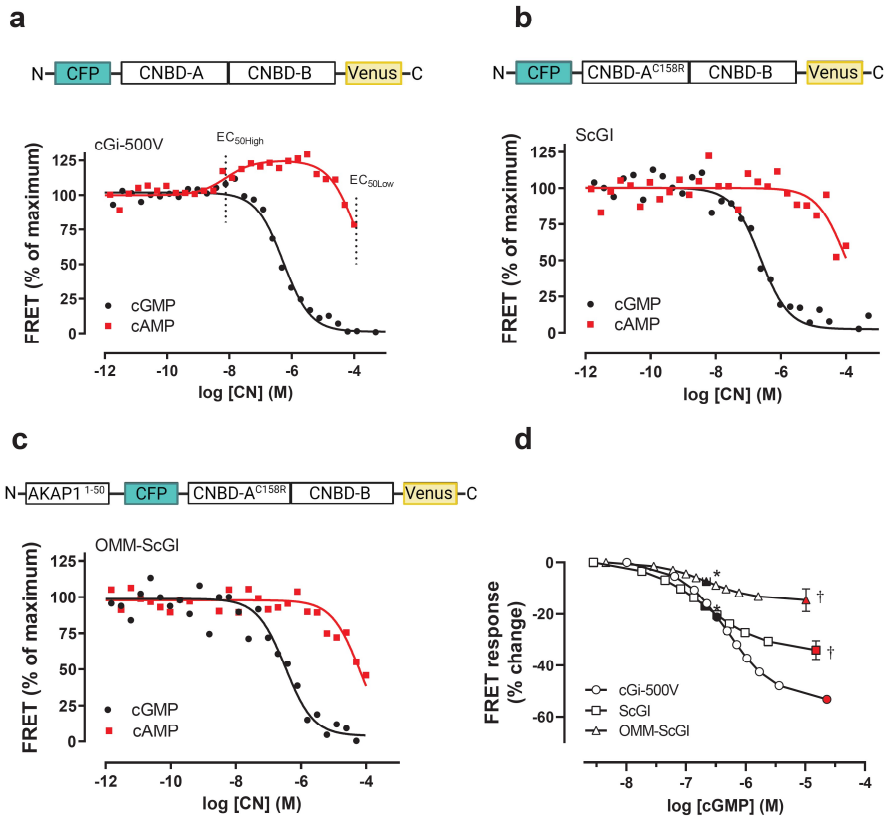

Figure 3. Development of FRET-based biosensor selective for cGMP and targeted to mitochondria. a-c) Upper panels: schematic of the indicated biosensor consisting of the fluorescent proteins CFP and Venus flanking the two cyclic nucleotide binding domains from PKG I without (cGi-500V) or with (ScGI) the C158R mutation. The OMM-ScGI contains an AKAP1 targeting sequence selective for the outer mitochondrial membrane. Lower panels: homogenates of HEK293 cells transfected with the indicated biosensor were incubated with increasing concentrations of either cGMP or cAMP. FRET (F_{Venus}/F_{CFP}) was measured as described in Materials and Methods and normalized to FRET in the absence of cGMP and at the highest cGMP concentration. Shown are representative of 10 (cGMP) and 5 (cAMP) independent experiments in **a**, 15 (cGMP) and 6 (cAMP) in **b**, 5 (cGMP) and 5 (cAMP) in **c. d)** Concentration-response curves generated by increasing concentrations of cGMP in homogenates of HEK293 cells expressing the indicated biosensors, as shown in a, b and c. EC_{50} values (marked as black filled symbols) and maximal change in FRET (marked as red filled symbols) are shown as mean±SEM from 12, 17 and 5 independent experiments for cGi-500V, ScGI and OMM-ScGI, respectively. *$p<0.001$ for pEC_{50} of ScGI or OMM-ScGI vs. cGI-500V; †$p< 0.0001$ for maximal FRET change of ScGI or OMM-ScGI vs. cGi-500V (one-way ANOVA, Sidak's test).

Figure 4

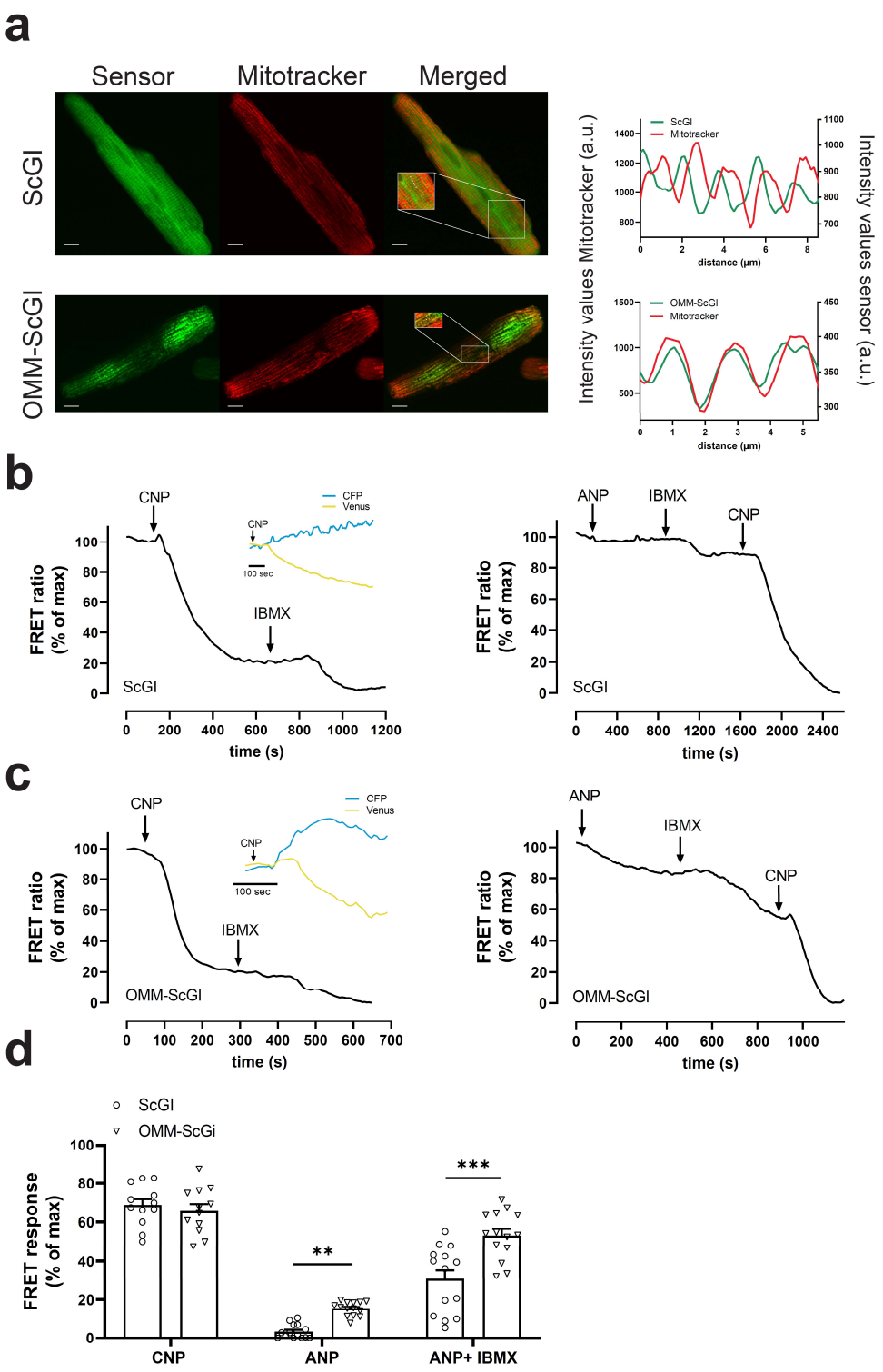

Figure 4. CNP and ANP increase cGMP at the outer mitochondrial membrane in cardiomyocytes. a) Cells expressing the ScGI (upper panel) and OMM-ScGI (lower panel),

773 were stained with Mitotracker Deep Red, washed and visualized under a confocal microscope
774 as described in Materials and Methods. Scale bar: 10µm. Right panels show colocalization by
775 intensity overlay of both fluorescent signals (Mitotracker and sensors) from indicated dotted
776 bar. a.u.: Arbitrary units **b and c)** Representative FRET ratio (Venus/CFP) recordings in single
777 cells expressing the indicated biosensor and stimulated with CNP (300nM) and IBMX (100µM)
778 (left panels) or ANP (1µM) followed by maximal activation of the biosensor (IBMX 100µM +
779 CNP 300 nM) (right panels). The inserts in the left panels show corresponding traces of
780 separate Venus and CFP intensities upon stimulation with CNP (300 nM). Shown are traces
781 representative of 10-14 cells from 5-8 independent experimtents **d)** Quantification of FRET
782 responses from stimulation with CNP, ANP or combined response of IBMX + ANP. **$p<0.01$
783 and ***$p<0.001$ (one-way ANOVA, Sidak's test).

784

Figure 5

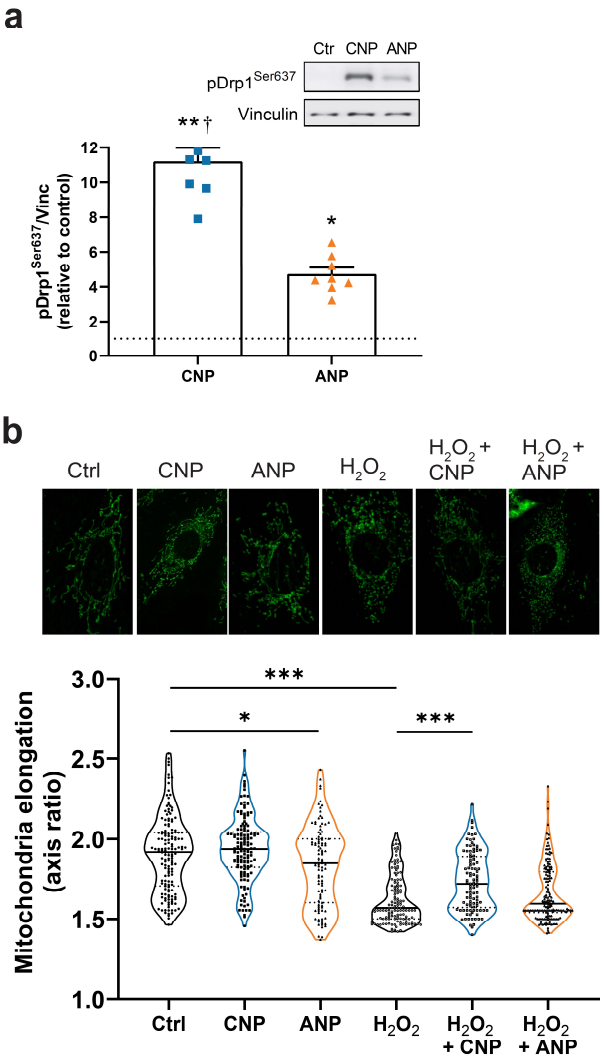

Figure 5. NPs modulate Drp1 phosphorylation and prevent mitochondrial fragmentation. a) Adult rat cardiomyocytes were stimulated with vehicle (H_2O; Ctr), CNP (1 µM) or ANP (1 µM) for 3 h and lysed. Phosphorylation of Drp1 at Ser637 ($pDrp1^{Ser637}$) was determined as described in Materials and Methods. The insert shows rrepresentative western blots of 5 independent experiments. The bands were quantified and normalized to loading control (vinculin) and Ctr (mean±SEM, n=5). *p< 0.05 and **p<0.01 *vs*. Ctr; †p<0.01 CNP *vs*. ANP (one-way ANOVA with Tukey's test). **b)** H9c2 cells were stained with Mitotracker Green, washed and visualized under a confocal microscope and pictures processed by ImageJ to obtain the mitochondrial elongation as described in Materials and Methods. Data are shown as mean±SEM of 102-158 cells from 4 independent experiments. *p<0.05, ***p<0.001 (one-way ANOVA, Sidak's multiple comparisons test).

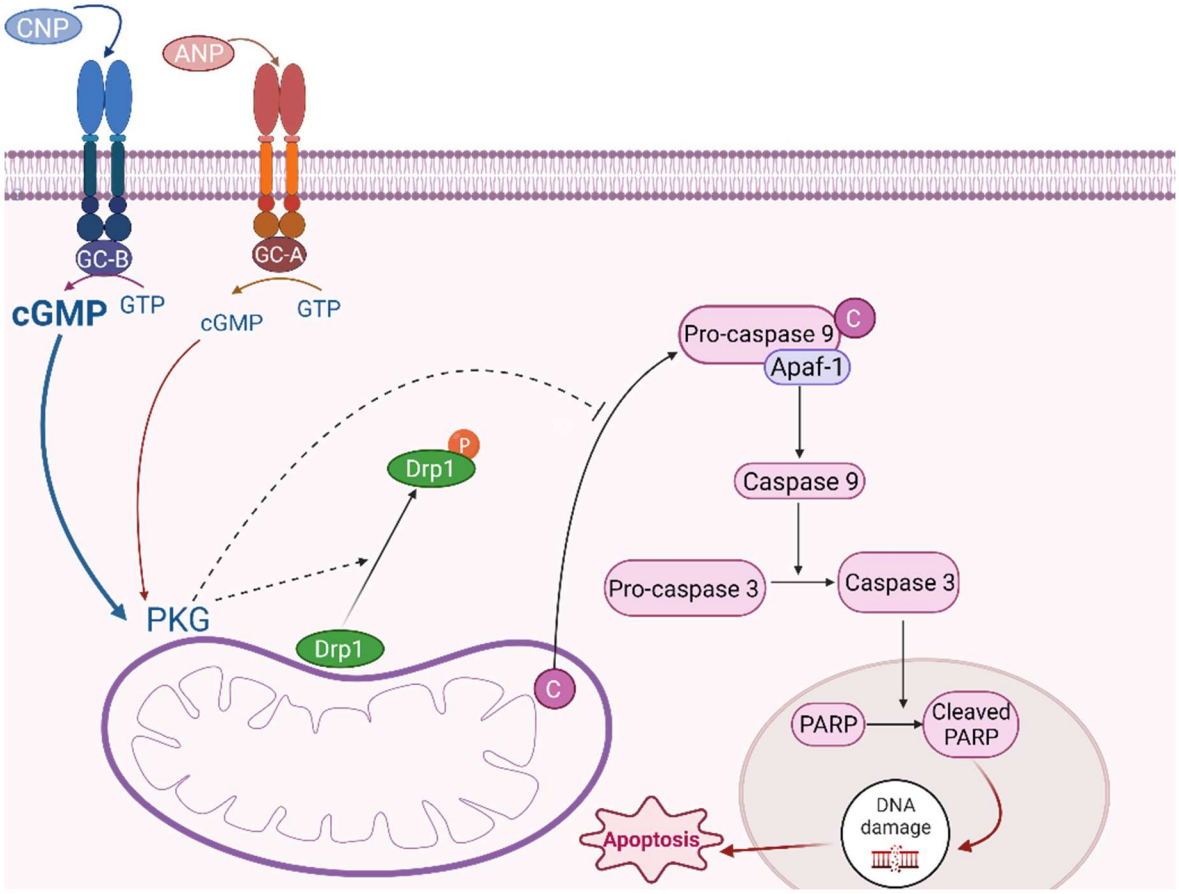

Figure 6. Natriuretic peptides reduce cardiomyocyte apoptosis through the mitochondrial intrinsic pathway by increasing cGMP at the OMM and increasing Drp1 phosphorylation. GC-A and GC-B stimulation by ANP and CNP respectively, generates cGMP differently in the cytosol and at the OMM, with the CNP-stimulated cGMP pool being greater than the ANP-stimulated cGMP pool. cGMP can activate PKG and mediate Drp1 phosphorylation, preventing its activation and its pro-apoptotic function at the OMM. ANP and CNP reduce cytochrome c release from the mitochondria, decreasing caspase 9 activation and the progression in apoptosis (PARP cleavage), while only CNP can prevent mitochondrial fragmentation. Dotted lines indicate suggested pathways. This figure was produced using Biorender.